Journal of Optics

PAPER

Radial Schmidt mode detector of entangled photons

To cite this article: Radhika Prasad *et al* 2026 *J. Opt.* **28** 075201

IOP Publishing J. Opt. 28 (2026) 075201 https://doi.org/10.1088/2040-8986/ae84e4

Journal of Optics

RECEIVED
24 February 2026

REVISED
26 May 2026

ACCEPTED FOR PUBLICATION
1 July 2026

PUBLISHED
27 July 2026

PAPER

Radial Schmidt mode detector of entangled photons

Radhika Prasad[1,*], **Nilakshi Senapati**[1], **Abhinandan Bhattacharjee**[2] and **Anand K Jha**[1,*]

[1] Department of Physics, Indian Institute of Technology Kanpur, Kanpur, UP 208016, India
[2] Universität Paderborn, Warburger Strasse 100, 33098 Paderborn, Germany
[*] Authors to whom any correspondence should be addressed.

E-mail: radhikap@iitk.ac.in and akjha@iitk.ac.in

Keywords: Schmidt spectrum, SPDC, OAM, entanglement

Abstract

High-dimensional spatially entangled two-photon states generated by the spontaneous parametric down-conversion process (SPDC) have become a promising resource for several quantum information science applications. In order to harness high-dimensional entanglement advantages, detection capability in the Schmidt basis is a necessity. Spatial entanglement has been explored in several modal bases, such as pixel, azimuthal, and radial modes. Among them, pixel and azimuthal entanglement have been widely utilized due to efficient access to their Schmidt modes, while radial-mode entanglement remains underexploited. This is due to radial coordinates not having a Schmidt-decomposed form for the SPDC photons or a technique for measuring high-dimensional radial Schmidt modes, which is a major roadblock in harnessing radial mode advantages. In this work, we first theoretically show that azimuthal averaging of SPDC two-photon states yields a radial Schmidt-decomposed form under typical experimental situations. We then demonstrate an innovative approach for extracting the radial Schmidt modes and their spectrum by characterizing the density matrix in the radial basis of one of the SPDC photons. Finally, we report the first-ever measurement of the radial Schmidt spectrum of up to 50 radial Schmidt modes with about 98% fidelity.

1. Introduction

High-dimensional entangled two-photon states offer benefits for quantum information applications, including increased information capacity [1], higher security [2], error tolerance [3], robustness to noise [4], supersensitive measurements [5], and teleportation [6]. Among all the potential degrees of freedom available for harnessing the high-dimensional benefits, such as time-energy [7] and pixel entanglement [8], the spatial entanglement of the signal and idler photons produced by spontaneous parametric down-conversion (SPDC) is the most suitable for quantum information applications [9]. This is because the spatial degree of freedom involves a complete set of discrete and infinite-dimensional modes that are usually propagating solutions to the wave equation, such as the Laguerre–Gaussian LG_p^l modes [10]. These modes are characterized by two indices, namely, the azimuthal and the radial. The most often used azimuthal modes are characterized by $e^{il\phi}$ phase dependence and contain $l\hbar$ orbital angular momentum (OAM) per photon, while the radial modes quantify the radial dependence of the field. Most works on radial modes have been with the so-called p-modes with several potential applications [11, 12]. The p-modes based two-photon entangled states have led to violations of Bell inequalities [13], the uncertainty principle for radial degrees of freedom [14], and realization of the Einstein–Podolsky–Rosen correlations [15].

In the last two decades, great effort has gone into generating and detecting high-dimensional entangled two-photon states using SPDC. However, harnessing high-dimensional advantages has been challenging due to the lack of suitable spatial-mode detectors for one-photon fields and spatial Schmidt-mode detectors for entangled two-photon fields. Schmidt modes are the modes in the basis in which the two-photon state has a Schmidt decomposed form, and it is very useful for quantifying and accessing high-dimensional entanglement [16]. An ideal detector for any basis is a mode sorter that spatially separates modes based on their mode index. In the azimuthal basis, the current sorter implementations involve either multiple diffractive elements and suffer from losses that are very difficult to estimate [17, 18], or sort OAM modes with substantial cross-talk [19]. In the absence of an OAM sorter, the other approach so far has been the projective measurement using a spatial light modulator (SLM) and a single mode fiber (SMF) [20, 21], but this approach suffers from mode-dependent losses. More recently, another viable approach has been developed that is based on reconstructing the OAM-mode spectrum by measuring the angular coherence function [22–25]. This has resulted in OAM-mode detectors that work for a broad range of modes and have a uniform detection efficiency over the entire range [24, 26].

Unlike azimuthal modes for which efficient mode detectors do exist, there is currently no such detector for radial modes. The current p-mode sorter implementations can sort either only a set of three pre-specified modes [27] or based on whether $l+p$ is odd or even [28]. Efforts based on projective measurements, involving an SLM and an SMF, have so far yielded a detector that works for only four radial modes with a very poor efficiency [29] and another detector that has been demonstrated to be efficient for only up to eight modes [30]. Thus, we note that the current advancement in radial-mode detection is still in the nascent stage. Furthermore, the reconstruction-based approach which has resulted in near-perfect OAM detectors [22–25, 31] has so far not been tried for radial modes.

In this work, we show that the azimuthally-averaged SPDC two-photon state can be approximated as a pure state under typical experimental situations. We thus derive a Schmidt-decomposed form in radial coordinates. Next, we propose a technique for reconstructing the radial-mode spectrum by measuring the azimuthally-averaged radially quasi-homogeneous coherence function and thereby demonstrate an experimental technique for measuring up to 50 radial Schmidt modes with about 98% fidelity.

2. Theory

The Laguerre–Gaussian (LG) modes, represented as $\mathrm{LG}_p^l(\rho,\theta)$, are exact solutions to the paraxial Helmholtz equation. The index l measures the OAM of each photon in units of $\hbar$, while the index p characterizes the radial variation in the intensity [10]. These modes form a complete basis, and any electric field $E(\rho,\theta)$ can be represented in terms of the projections over them:

$$E(\boldsymbol{\rho}) = \sum_{l,p} A_{lp}\mathrm{LG}_p^l(\boldsymbol{\rho}) = \sum_{l,p} A_{lp}\mathrm{LG}_p^l(\rho)\,\mathrm{e}^{\mathrm{i}l\theta}, \tag{1}$$

where A_{lp} are superposition coefficients, and $\boldsymbol{\rho} \equiv (\rho,\theta)$ is the transverse position vector in the cylindrical coordinates. In the projective measurement of OAM modes, one essentially measures coefficients A_{lp}, quite often with $p=0$ [20, 21]. In the context of the SPDC process, a pump photon at a higher frequency down-converts into two photons at lower frequencies, referred to as the signal and idler. The state of the down-converted photons is given by:

$$|\psi_{si}\rangle = \iint \psi_{si}(\boldsymbol{\rho}_s,\boldsymbol{\rho}_i)\,|\boldsymbol{\rho}_s\rangle|\boldsymbol{\rho}_i\rangle \mathrm{d}^2\boldsymbol{\rho}_s \mathrm{d}^2\boldsymbol{\rho}_i, \tag{2}$$

where under the Gaussian approximation for collinear phase-matching condition, $\psi_{si}(\boldsymbol{\rho}_s,\boldsymbol{\rho}_i)$ is given by [32–34]:

$$\psi_{si}(\boldsymbol{\rho}_s,\boldsymbol{\rho}_i) = A\exp\left[-\frac{(\boldsymbol{\rho}_s+\boldsymbol{\rho}_i)^2}{4w_p^2}\right]\exp\left[-\frac{(\boldsymbol{\rho}_s-\boldsymbol{\rho}_i)^2}{4\sigma_-^2}\right]. \tag{3}$$

Here, A is the normalization constant and the subscripts p, s, and i stand for pump, signal and idler, respectively; w_p is the beam-waist width of the pump and $\sigma_-^2 = \frac{L\lambda_p}{6\pi}$, where L is the crystal length and λ_p is the pump wavelength [32]. In order to study the spatial entanglement properties of SPDC photons, the two-photon state $|\psi_{si}\rangle$ is often expressed in the LG basis as [20, 35]:

$$|\psi_{si}\rangle = \sum_{l_s}\sum_{p_s}\sum_{l_i}\sum_{p_i} C_{l_s,p_s}^{l_i,p_i}|l_s,p_s\rangle_s|l_i,p_i\rangle_i. \tag{4}$$

where l_p is the OAM mode index of the pump photon, and $|l_s,p_s\rangle_s$ represents the state of the signal photon with indices l_s and p_s, etc. Using equations (2) and (4), we get

$$C_{l_s,p_s}^{l_i,p_i} = \iint \psi_{si}(\boldsymbol{\rho}_s,\boldsymbol{\rho}_i)\,\mathrm{LG}_{p_s}^{l_s*}(\boldsymbol{\rho}_s)\,\mathrm{LG}_{p_i}^{l_i*}(\boldsymbol{\rho}_i)\,\mathrm{d}^2\boldsymbol{\rho}_s\mathrm{d}^2\boldsymbol{\rho}_i. \tag{5}$$

We note that equation (4) involves summations over four indices. As a result, it is not in the Schmidt-decomposed form [16], since that should involve summations over only two indices. However, for efficiently harnessing and quantifying entanglement, expressing a state in the Schmidt basis and having the detection capability in that basis is a must.

2.1. Azimuthal (OAM) Schmidt spectrum of SPDC photons

We note that for most of the works related to OAM entanglement, one is not interested in the radial dependence of the field and that OAM measurements are restricted either to $p_s = p_i = 0$ modes [20] or is averaged over all the radial modes [24–26]. For such measurement scenarios, the state of the two-photon field for a Gaussian pump field ($l_p = 0$) is assumed to be [20]:

$$|\psi_{si}^{(\mathrm{az})}\rangle = \sum_{l} \sqrt{C_l} |l\rangle_s |-l\rangle_i, \tag{6}$$

which is a Schmidt-decomposed form in the OAM basis. Although this form has not been derived rigorously, it is widely used and has been verified in experiments to a good approximation. In equation (6), C_l is referred to as the OAM Schmidt spectrum, and it represents the probability that the signal and idler photons have OAM $l\hbar$ and $-l\hbar$, respectively. From equation (6), the density matrix element corresponding to the signal photon field can be obtained by taking the partial trace over the idler photon:

$$\left\langle \theta_s \middle| \mathrm{Tr}_i \left[\left| \psi_{si}^{(\mathrm{az})} \right\rangle \langle \psi_{si}^{(\mathrm{az})} \right| \right] \left| \theta_s' \right\rangle = \frac{1}{2\pi} \sum_{l} C_l e^{il\left(\theta_s - \theta_s'\right)} \equiv W_s^{(\mathrm{az})}\left(\theta_s, \theta_s'\right). \tag{7}$$

The density matrix element $W_s^{(\mathrm{az})}(\theta_s, \theta_s')$ can also be referred to as the angular coherence function of the signal field. The above equation is the coherent mode decomposition of the signal field [22, 37]. Since C_l is the weightage of the OAM modes, it is referred to as the OAM spectrum. Thus, from equations (6) and (7), we can see that the OAM spectrum of one of the down-converted photons is the same as the OAM Schmidt spectrum of the entangled two-photon field [22]—this fact is used for experimentally measuring the OAM Schmidt spectrum [23–26].

2.2. Radial Schmidt spectrum of SPDC photons

Next, we work out an analogous technique for measuring the radial Schmidt spectrum of entangled two-photon fields. In the radial coordinates, the measurement techniques have so far demonstrated measuring radial modes only as p-modes, and up to $p = 8$ for single photon states [27–30]. However, more recently, measurements of radial modes of entangled photons have also been demonstrated, through direct p-mode projective measurements [13] and through interferometric reconstruction of the spatial biphoton state, from which the p-mode spectrum was subsequently extracted [38]. To the best of our knowledge, the Schmidt-decomposed form in radial coordinates has neither been derived analytically nor is there any experimental technique for measuring it. To represent the two-photon state in terms of only radial variables (ρ_s, ρ_i), we take the partial trace of $|\psi_{si}\rangle$ in equation (2) over the azimuthal variables (θ_s, θ_i). This yields a two-photon state, the density matrix element of which can be written as

$$W_{si}^{(\mathrm{rad})}\left(\rho_s, \rho_i, \rho_s', \rho_i'\right) = \iint \psi_{si}^{*}\left(\boldsymbol{\rho}_s', \boldsymbol{\rho}_i'\right) \psi_{si}\left(\boldsymbol{\rho}_s, \boldsymbol{\rho}_i\right) \mathrm{d}\theta_s \mathrm{d}\theta_i. \tag{8}$$

$W_{si}^{(\mathrm{rad})}\left(\rho_s, \rho_i, \rho_s', \rho_i'\right)$ can also be referred to as the two-photon radial cross-spectral density function [39]. We consider the state to be normalized, that is, $\mathrm{Tr}\left[\left[W_{si}^{(\mathrm{rad})}\left(\rho_s, \rho_i, \rho_s', \rho_i'\right)\right]\right] = 1$, where $[\cdots]$ denotes matrix representation. We note that the Schmidt decomposition for a two-photon state exists only if the state is pure and that the state represented by equation (8) is strictly speaking a mixed state. However, if the mixedness of this state is negligible or in other words if the purity of the state is close to unity, we can take the state to be pure, which will then have a Schmidt decomposition. A generic quantifier of the purity of any quantum state is the intrinsic degree of coherence, represented by P_∞ for continuous variable bases, such as position, momentum, etc, P_∞ is defined as $P_\infty = \mathrm{Tr}[\rho^2]$, where ρ is the density matrix of the quantum state [36, 40]. And, therefore, for the above state we have, $P_\infty = \mathrm{Tr}[\rho^2] = \left[\left[W_{si}^{(\mathrm{rad})}\left(\rho_s, \rho_i, \rho_s', \rho_i'\right)\right]^2\right]$. P_∞ ranges from 0 to 1, with $P_\infty = 1$ representing a pure state and $P_\infty = 0$ representing the completely mixed state. Using equations (3) and (8), we evaluate P_∞ for various values of the crystal length L and the pump beam waist w_p for $\lambda_p = 355$ nm. Figure 1 plots P_∞ as a function of L and w_p. We find that as a function of w_p, P_∞ remains unchanged, whereas P_∞ increases as

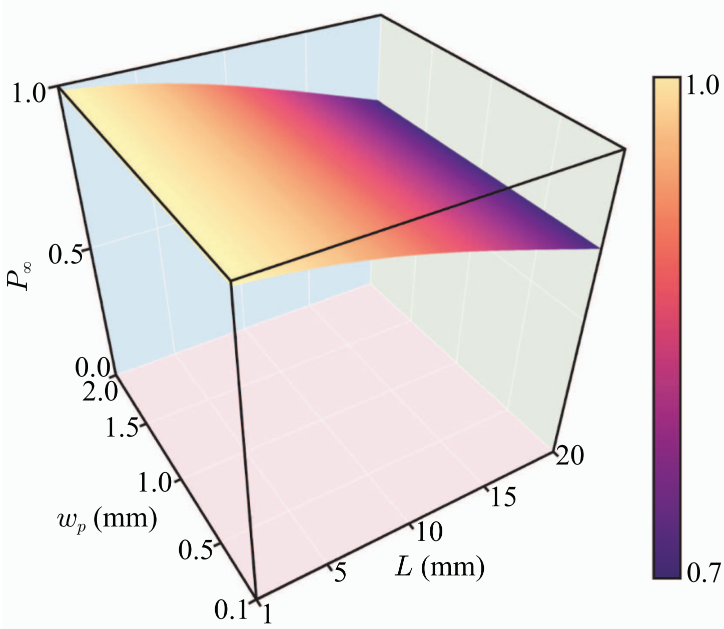

Figure 1. Numerical plot of the purity P_∞ of the two-photon state $W_{si}^{(\mathrm{rad})}(\rho_s,\rho_i,\rho_s',\rho_i')$ as a function of crystal length L and beam waist w_p. The purity is defined as $P_\infty \equiv \mathrm{Tr}\left[\left[W_{si}^{(\mathrm{rad})}(\rho_s,\rho_i,\rho_s',\rho_i')\right]^2\right]$ [36]. $P_\infty = 1$ represents a pure state while $P_\infty = 0$ represents a completely mixed state. We see that as a function of the beam waist w_p, P_∞ remains unchanged, whereas it decreases as the crystal length L increases.

L decreases. Thus, we see that as the crystal becomes thinner, P_∞ approaches unity. In our experiments reported below, we employ crystals with $L = 1$ mm and $L = 5$ mm, for which the P_∞ comes out to be 0.98 and 0.95, respectively. More importantly, as we show in the experimental section, for producing a high-dimensional radial Schmidt spectrum, one requires a thinner crystal. Therefore, in the case of higher-dimensional Schmidt spectrum, the accuracy of this approximation becomes progressively better. Thus, for such crystal lengths, we approximate P_∞ to be unity and take the state represented by equation (8) to be pure, and we therefore write the density matrix element of equation (8) as $W_{si}^{(\mathrm{rad})}(\rho_s,\rho_i,\rho_s',\rho_i') \approx \psi_{si}^{*(\mathrm{rad})}(\rho_s,\rho_i)\,\psi_{si}^{(\mathrm{rad})}(\rho_s',\rho_i')$, where $\psi_{si}^{(\mathrm{rad})}(\rho_s,\rho_i)$ represents a pure two-photon wavefunction, which must have a Schmidt-decomposed form that can be represented as

$$\psi_{si}^{(\mathrm{rad})}(\rho_s,\rho_i) = \sum_n \sqrt{\lambda_n}\phi_n^{(s)}(\rho_s)\,\phi_n^{(i)}(\rho_i). \tag{9}$$

Here, λ_n can be referred to as the radial Schmidt spectrum and $\phi_n^{(s)}(\rho_s)$ as the radial Schmidt modes. We consider the SPDC phase matching to be low-gain, degenerate, and type-I collinear, in which case the eigenfunctions $\phi_n^{(s)}(\rho_s)$ and $\phi_n^{(i)}(\rho_i)$ will have the same functional form. Equation (9) can be referred to as the radial Schmidt decomposition of the entangled two-photon field, and it is analogous to the azimuthal Schmidt decomposition given in equation (6). From the two-photon state in equation (9), the state of the signal photon can be calculated by taking the partial trace over the idler. Thus, the density matrix element corresponding to the signal photon in the radial basis can be shown to be:

$$\begin{aligned} W_s^{(\mathrm{rad})}(\rho_s,\rho_s') &= \int \psi_{si}^{*(\mathrm{rad})}(\rho_s',\rho_i)\,\psi_{si}^{(\mathrm{rad})}(\rho_s,\rho_i)\,\mathrm{d}\rho_i \\ &= \sum_n \lambda_n \phi_n^{*(s)}(\rho_s')\,\phi_n^{(s)}(\rho_s). \end{aligned} \tag{10}$$

We note that $W_s^{(\mathrm{rad})}(\rho_s,\rho_s')$ can be referred to as the radial cross-spectral density function corresponding to the signal photon, and it quantifies coherence in the radial coordinates [41]. Furthermore, $W_s^{(\mathrm{rad})}(\rho_s,\rho_s')$ in equation (10) is the coherent mode representation [41, 42], and, therefore, λ_n in the above equation represents the radial-mode spectrum of the signal photon, just as C_l represents the OAM-mode spectrum in equation (7). Comparing equations (9) and (10), we find that the radial Schmidt spectrum of the entangled two-photon field is the same as the radial-mode spectrum of either

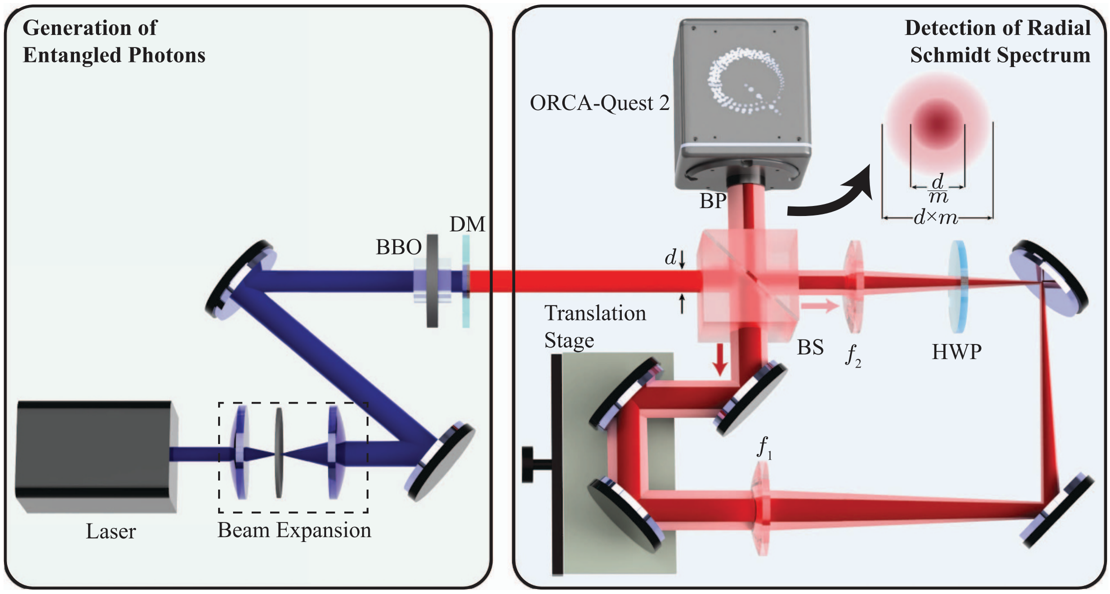

Figure 2. Experimental setup involving a common-path Sagnac interferometer. Laser: ultraviolet (UV) laser; BS: beam splitter; BBO: β-Barium Borate crystal; HWP: half-wave plate (optic axis orientation ϕ kept at 0 and $\pi/4$ radians from the horizontal); DM: dichroic mirror; BP: bandpass filter. We represent the reflected and transmitted beams at the BS with different colors (dark red and light red, respectively) to highlight the magnification due to $4f$ lens configuration. The BBO crystal is used for the generation of entangled photons and the interferometer detects the radial Schmidt spectrum.

the signal or the idler photon. Equation (10) is the main theoretical result of this work, which implies that by measuring the radial cross-spectral density function $W_s^{(\mathrm{rad})}(\rho_s,\rho_s')$ and then finding its coherent mode representation, one can obtain the radial Schmidt spectrum λ_n and the corresponding Schmidt modes $\phi_n(\rho_s)$ of the entangled two-photon states. We note that, unlike equation (6), in which case the Schmidt modes are assumed to be the OAM modes, the functional form of the Schmidt modes has not been assumed in equation (10) but is obtained through the coherent mode representation of the experimentally measured $W_s^{(\mathrm{rad})}(\rho_s,\rho_s')$. Thus, our method works for any radial-mode bases and not just the p-modes which have been the subject of investigation in most prior works [27–30].

3. Experimental measurement scheme

Figure 2 shows the experimental setup, involving a Sagnac-type interferometer. The interferometer measures any cross-spectral density function $W_s(\boldsymbol{\rho}_s,\boldsymbol{\rho}_s')$ that is quasi-homogeneous [42], or in other words, any $W_s(\boldsymbol{\rho}_s,\boldsymbol{\rho}_s')$ that can be expressed as

$$W(\boldsymbol{\rho}_s,\boldsymbol{\rho'}_s)=\sqrt{I(\boldsymbol{\rho}_s)I(\boldsymbol{\rho'}_s)}\mu(\boldsymbol{\rho}_s-\boldsymbol{\rho'}_s). \tag{11}$$

Here, $I(\boldsymbol{\rho}_s)=W(\boldsymbol{\rho}_s,\boldsymbol{\rho}_s)$ is the transverse position probability of the signal photon and $\mu(\boldsymbol{\rho}_s-\boldsymbol{\rho'}_s)$ represents the degree of spatial coherence between $\boldsymbol{\rho}_s$ and $\boldsymbol{\rho'}_s$. The quasi-homogeneity condition requires that (i) the width of $\mu(\boldsymbol{\rho}_s-\boldsymbol{\rho'}_s)$ must be much smaller than the width of $I(\boldsymbol{\rho}_s)$ and (ii) $\mu(\boldsymbol{\rho}_s-\boldsymbol{\rho'}_s)$ should depend only on the difference coordinate $\boldsymbol{\rho}_s-\boldsymbol{\rho'}_s$. Given the two-photon wavefunction in equation (2), it can be numerically shown that for type-I, collinear, degenerate SPDC process for which $\sigma_-\ll w_p$ [33], the functional form of $W(\boldsymbol{\rho}_s,\boldsymbol{\rho'}_s)$ is that of a radial Gaussian Schell-model beam [41, 42], which is an example of a quasi-homogeneous field.

The interferometer of figure 2 consists of $4f$ lens configuration for magnification and a half-wave plate (HWP) for phase control. The field gets magnified by a factor of $m=f_1/f_2$ in alternative one (light red, transmitted twice at the beam splitter) and demagnified by the same factor m in alternative two (dark red, reflected twice at the beam splitter). The detection probability $I_{\mathrm{out}}^{\phi}(\boldsymbol{\rho}_s)$ at the camera plane is given by (for details see reference [42]):

$$I_{\mathrm{out}}^{\phi}(\boldsymbol{\rho}_s)=I_{\mathrm{out}}^{\phi}(\rho_s,\theta_s)=I(m\rho_s,\theta_s)+I\left(\frac{\rho_s}{m},\theta_s\right)-2W\left(m\rho_s,\theta_s;\frac{\rho_s}{m},\theta_s\right)\cos(4\phi), \tag{12}$$

where ϕ is the HWP angle with respect to the horizontal axis. Here, we have taken the beam splitter to be 50:50 and the cross-spectral density function $W\left(m\rho_s,\theta_s;\frac{\rho_s}{m},\theta_s\right)$ to be real. $I\left(m\rho_s,\theta_s\right)$ and $I\left(\frac{\rho_s}{m},\theta_s\right)$ are the detection probabilities of the individual interfering paths. We note that $W\left(m\rho_s,\theta_s;\frac{\rho_s}{m},\theta_s\right))$ can be measured by recording $I_{\text{out}}^{\phi}\left(\rho_s,\theta_s\right)$ at $\phi=0$ and $\phi=\pi/4$, that is, $W\left(m\rho_s,\theta_s;\frac{\rho_s}{m},\theta_s\right))=\frac{1}{4}\left[I_{\text{out}}^{\phi=\pi/4}(\rho_s,\theta_s)-I_{\text{out}}^{\phi=0}(\rho_s,\theta_s)\right]$, and thereby the radial cross-spectral density function of the signal photon can be obtained as

$$W_s^{(\text{rad})}\left(m\rho_s,\frac{\rho_s}{m}\right)=\frac{1}{2\pi}\int_{-\pi}^{\pi}W\left(m\rho_s,\theta_s;\frac{\rho_s}{m},\theta_s\right)\mathrm{d}\theta_s. \tag{13}$$

For measuring $I(m\rho_s)$ and $I\left(\frac{\rho_s}{m}\right)$, one needs to remove the beam splitter from the interferometer. In this way, a field from only one interfering path reaches the camera and thus one measures $I\left(\frac{\rho_s}{m}\right)$. Since it is a common path interferometer, one cannot directly measure $I(m\rho_s)$, but it can be assessed by rescaling the measured $I\left(\frac{\rho_s}{m}\right)$ by the factor m. The degree of coherence function can therefore be obtained as

$$\mu_s^{(\text{rad})}\left(m\rho_s,\frac{\rho_s}{m}\right)=\frac{W_s^{(\text{rad})}\left(m\rho_s,\frac{\rho_s}{m}\right)}{\sqrt{I(m\rho_s)I(\frac{\rho_s}{m})}}. \tag{14}$$

Now, by utilizing the quasi-homogeneity of the field, we write: $\mu_s^{(\text{rad})}\left(m\rho_s,\frac{\rho_s}{m}\right)=\mu_s^{(\text{rad})}\left(m\rho_s-\frac{\rho_s}{m}\right)=\mu_s^{(\text{rad})}\left[\rho_s\left(m-\frac{1}{m}\right)\right]$. Thus, from the experimental measurements, one can obtain $\mu_s^{(\text{rad})}\left(m\rho_s-\frac{\rho_s}{m}\right)$ for a given value of m. We note that the degree of coherence function obtained in this way depends only on one variable, $\rho_s\left(m-\frac{1}{m}\right)$. However, the degree of coherence function is a two-point correlation function. Thus, from the measured values of $\mu_s^{(\text{rad})}\left[\rho_s\left(m-\frac{1}{m}\right)\right]$, one can obtain the two-point degree of coherence function $\mu_s^{(\text{rad})}(\rho,\rho')$ by realizing that the value of $\mu_s^{(\text{rad})}(\rho,\rho')$ for each pair of (ρ,ρ') is related to the single-variable $\mu_s^{(\text{rad})}(\rho-\rho')$ by $\mu_s^{(\text{rad})}(\rho,\rho')=\mu_s^{(\text{rad})}(\rho-\rho')$. Once $\mu_s^{(\text{rad})}(\rho,\rho')$ is numerically reconstructed, one can numerically obtain the cross-spectral density function $W_s^{(\text{rad})}(\rho,\rho')$ using equation (14). By numerically diagonalizing $W_s^{(\text{rad})}(\rho,\rho')$, one can finally obtain the radial coherent modes and radial mode spectrum of equation (10) and thus the radial Schmidt modes of equation (9).

4. Experimental setup

Figure 2 shows the experimental setup. A continuous wave ultraviolet (UV) laser of wavelength 355 nm pumps a type-I β-barium borate (BBO) crystal to generate collinear degenerate SPDC photons centered at a wavelength of 710 nm. We perform experiments with two different pump beam waists, w_p =507 μm and 1014μm. We use a lens combination after the pump laser to achieve the desired pump beam waist at the crystal plane. A dichroic mirror (DM) is kept just after the crystal to block the UV pump and transmit the signal and idler photons. In our experiments, we use two different lengths of the crystal, $L=5$ mm and $L=1$ mm, for which P_∞ comes out to be 0.95 and 0.98, such that the two-photon state in equation (8) can be approximated to be pure. We note that the signal and idler fields generated by SPDC co-propagate through the interferometer. The interferogram recorded by the camera is the sum of the intensity distributions of the signal field and idler field at the camera plane. For type-I degenerate SPDC, the signal and idler fields are spatially identical, that is, both the signal and idler fields have identical intensity distributions at the camera plane. Therefore, the recorded interferogram is equivalent to that produced by either the signal or the idler photon. The down-converted field enters the interferometer shown in figure 2 and the interference pattern is recorded by an ORCA-Quest 2 qCMOS camera. For the 4f imaging system inside the interferometer, we use lenses with focal lengths $f_1=400$ mm and $f_2=200$ mm, and thus in our experiments we have $m=2$. A translation stage is introduced to ensure that the separation between the two lenses remains intact. A 10 nm bandpass filter centered at 710 nm is placed in front of the camera to ensure high temporal coherence of the detected field.

5. Results and discussions

Figure 3 shows the experimental data and the retrieved Schmidt spectra for three different settings of w_p and L. Figure 3(a) corresponds to $w_p=507\mu$m and $L=5$ mm; figure 3(b) corresponds to $w_p=507\mu$m and $L=1$ mm; figure 3(c) corresponds to $w_p=1014\mu$m and $L=1$ mm. For each setting, the sub-figure (i) shows the recorded interferograms at $\phi=\pi/4$ (constructive interference) and $\phi=0$ (destructive

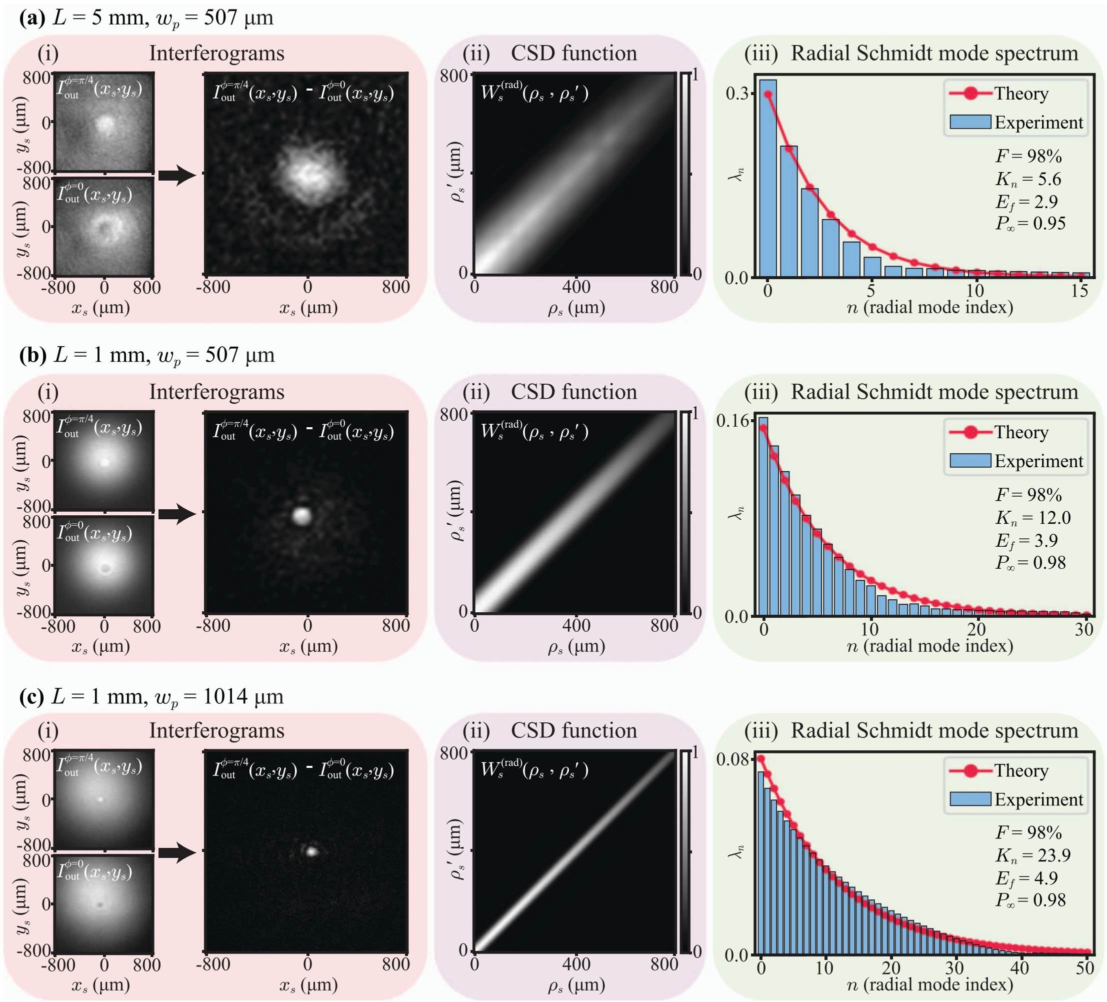

Figure 3. Experimental results: The radial Schmidt mode spectrum of entangled photons for different combinations of L and w_p. (a) $L = 5$ mm and $w_p = 507 \mu$m; (b) $L = 1$ mm and $w_p = 507 \mu$m; (c) $L = 1$ mm and $w_p = 1014 \mu$m. (i) Recorded interferograms at $\phi = \pi/4$ and $\phi = 0$, and their corresponding difference. (ii) The signal photon radial cross-spectral density (CSD) function $W_s^{(\mathrm{rad})}(\rho_s, \rho_s')$. (iii) The radial Schmidt mode spectrum obtained by finding eigenvalues of $W_s^{(\mathrm{rad})}(\rho_s, \rho_s')$. The red curve is the theoretical prediction and the blue bars are the experimentally obtained values. F is the fidelity, K_n is the Schmidt number, E_f is the entanglement of formation, and P_∞ is the two-photon state purity.

interference), along with their differences; the sub-figure (ii) presents the reconstructed radial cross-spectral density function $W_s^{(\mathrm{rad})}(\rho, \rho')$; and the sub-figure (iii) presents the normalized radial Schmidt spectrum of the entangled two-photon state. Along with the reconstructed radial Schmidt spectrum indicated by the blue histogram, the sub-figures (iii) show the theoretical predictions plotted in red. We find an excellent match between theory and experiment with a fidelity of 98% for all the reconstructed Schmidt spectra. The fidelity F characterizes the accuracy of the measurement, and is calculated as the similarity between the theoretical prediction and experimental measurement [35]. We note that the diagonal width of $W_s^{(\mathrm{rad})}(\rho, \rho')$ corresponds to the radial coherence width while the anti-diagonal width of $W_s^{(\mathrm{rad})}(\rho, \rho')$ is the radial width of the intensity of the field. We note that the diagonal width of $W_s^{(\mathrm{rad})}(\rho, \rho')$ decreases with the increasing w_p and decreasing L. And as $W_s^{(\mathrm{rad})}(\rho, \rho')$ decreases, the radial Schmidt spectrum becomes wider and the dimensionality of the state increases. We quantify the dimensionality of the state by evaluating the Schmidt number $K_n = 1/\sum_n \lambda_n^2$, which provides the effective number of radial modes contained by the SPDC state. We find that K_n increases from 5.6 to 23.9 as w_p increases and L decreases. This increasing trend in K_n is a qualitative signature of the increase of radial entanglement. This trend is also captured by the entanglement of formation E_f [43, 44], another entanglement certifier. A positive value of E_f implies the presence of entanglement [45]. In our case, E_f can be evaluated as $E_f = -\sum_n \lambda_n \log_2 \lambda_n$ [46]. The values of K_n and E_f are also shown in column figure 3(iii). The radial Schmidt modes corresponding to the three different settings of w_p and L are plotted in figure 4, which shows the first four mode profiles (dots) alongside their theoretical predictions (solid curve). We again see a very good match between the theoretical and experimental plots. Finally,

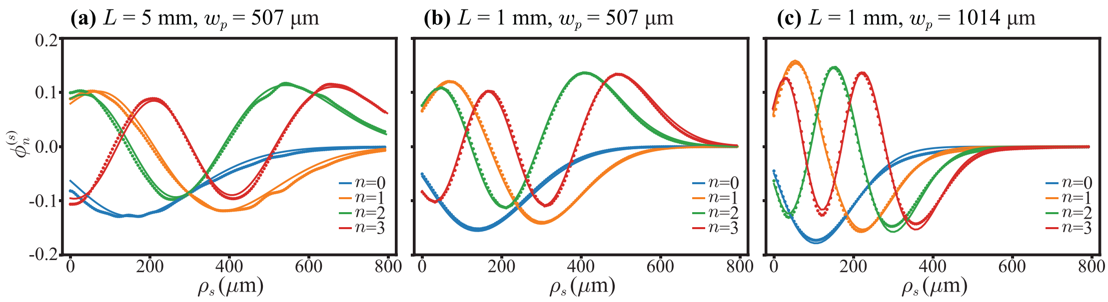

Figure 4. Schmidt modes for the three different experimental conditions: (a) $L = 5$ mm and $w_p = 507\mu$m; (b) $L = 1$ mm and $w_p = 507\mu$m; (c) $L = 1$ mm and $w_p = 1014\mu$m. The dotted lines are experimental measurements, while the solid lines are the theoretical predictions.

we note that since our scheme is based on a Sagnac interferometer, which is a common-path interferometer and is known not to suffer from typical interferometric stability issues, it is quite robust and thus works for high-dimensional states.

6. Conclusion

In this work, we show that the azimuthally averaged SPDC two-photon state can be well approximated as a radially pure two-photon state under typical experimental conditions, which allows us to derive a Schmidt-decomposed representation in radial coordinates for the entangled two-photon fields produced by SPDC under low-gain, degenerate, collinear type-I phase-matching condition. We then propose and demonstrate a scheme for reconstructing the radial Schmidt spectrum and modes by directly characterizing the density matrix in the radial basis of one of the SPDC photons. This method has enabled the measurements of up to 50 radial Schmidt modes with a fidelity of 98%. To the best of our knowledge, this represents at least a five-fold improvement in the detection capability of radial modes over existing radial-mode detectors. In contrast to most Schmidt-mode characterization schemes, our approach does not require coincidence measurements, which makes our approach accurate and resource efficient. Furthermore, the existing methods work only if the radial Schmidt basis is known a-priori whereas in our scheme the radial Schmidt basis is directly measured. Additionally, the technique is readily applicable to the characterization of the Schmidt spectrum of bright SPDC sources well beyond the photon-pair regime, which can be used to estimate squeezing of independent radial Schmidt modes. We therefore expect our method to have important implications for high-dimensional quantum information applications.

Acknowledgments

R.P and N.S. thank the Prime Minister's Research Fellowship (PMRF), Government of India, for financial support.

Data availability statement

All data that support the findings of this study are included within the article (and any supplementary files).

Funding

We acknowledge financial support from the Science and Engineering Research Board through grants STR/2021/000035 & CRG/2022/003070, and from the Department of Science & Technology, Government of India through the grant DST/ICPS/QuST/Theme-I/2019 and the National Quantum Mission (NQM) grant DST/FFT/NQM/QSM/2024/3 for the technical group (TG) project on quantum imaging.

ORCID iDs

Radhika Prasad 0000-0002-9748-5264
Nilakshi Senapati 0009-0008-8407-2883
Abhinandan Bhattacharjee 0000-0002-0646-2404
Anand K Jha 0000-0002-5186-6264

References

[1] Bozinovic N, Yue Y, Ren Y, Tur M, Kristensen P, Huang H, Willner A E and Ramachandran S 2013 Terabit-scale orbital angular momentum mode division multiplexing in fibers *Science* **340** 1545–8
[2] Cerf N J, Bourennane M, Karlsson A and Gisin N 2002 Security of quantum key distribution using d-level systems *Phys. Rev. Lett.* **88** 127902
[3] Bechmann-Pasquinucci H and Peres A 2000 Quantum cryptography with 3-state systems *Phys. Rev. Lett.* **85** 3313
[4] Zhu F, Tyler M, Valencia N H, Malik M and Leach J 2021 Is high-dimensional photonic entanglement robust to noise? *AVS Quantum Sci.* **3** 011401
[5] Jha A K, Agarwal G S and Boyd R W 2011 Supersensitive measurement of angular displacements using entangled photons *Phys. Rev. A* **83** 053829
[6] Luo Y-H *et al* 2019 Quantum teleportation in high dimensions *Phys. Rev. Lett.* **123** 070505
[7] Zhang D, Zhang Y, Li X, Zhang D, Cheng L, Li C and Zhang Y 2017 Generation of high-dimensional energy-time-entangled photon pairs *Phys. Rev. A* **96** 053849
[8] O'Sullivan-Hale M N, Khan I A, Boyd R W and Howell J C 2005 Pixel entanglement: experimental realization of optically entangled d = 3 and d = 6 qudits *Phys. Rev. Lett.* **94** 220501
[9] Yao A M and Padgett M J 2011 Orbital angular momentum: origins, behavior and applications *Adv. Opt. Photonics* **3** 161–204
[10] Allen L, Beijersbergen M W, Spreeuw R J C and Woerdman J P 1992 Orbital angular momentum of light and the transformation of Laguerre-Gaussian laser modes *Phys. Rev. A* **45** 8185–9
[11] Olvera-Santamaría M A and Ostrovsky A 2023 Synthesis of partially coherent bessel-mode vortex-beams with radial coherence *J. Opt.* **25** 095601
[12] Wang Y, Bai L, Xie J, Huang C and Guo L 2024 Radial spectrum spread of Laguerre-Gaussian beam transmission in weak compressible turbulence *Opt. Commun.* **554** 130111
[13] Zhang D, Qiu X, Zhang W and Chen L 2018 Violation of a bell inequality in two-dimensional state spaces for radial quantum number *Phys. Rev. A* **98** 042134
[14] Zhang Z, Zhang D, Qiu X, Chen Y, Franke-Arnold S and Chen L 2022 Experimental investigation of the uncertainty principle for radial degrees of freedom *Photon. Res.* **10** 2223–8
[15] Chen L, Ma T, Qiu X, Zhang D, Zhang W and Boyd R W 2019 Realization of the einstein-podolsky-rosen paradox using radial position and radial momentum variables *Phys. Rev. Lett.* **123** 060403
[16] Ekert A and Knight P L 1995 Entangled quantum systems and the schmidt decomposition *Am. J. Phys.* **63** 415–23
[17] Mirhosseini M, Malik M, Shi Z and Boyd R W 2013 Efficient separation of the orbital angular momentum eigenstates of light *Nat. Commun.* **4** 2781
[18] Berkhout G C G, Lavery M P J, Courtial J, Beijersbergen M W and Padgett M J 2010 Efficient sorting of orbital angular momentum states of light *Phys. Rev. Lett.* **105** 153601
[19] Sahu R, Chaudhary S, Khare K, Bhattacharya M, Wanare H and Jha A K 2018 Angular lens *Opt. Express* **26** 8709
[20] Mair A, Vaziri A, Weihs G and Zeilinger A 2001 Entanglement of the orbital angular momentum states of photons *Nature* **412** 313–6
[21] Heckenberg N, McDuff R, Smith C and White A 1992 Generation of optical phase singularities by computer-generated holograms *Opt. Lett.* **17** 221–3
[22] Jha A K, Agarwal G S and Boyd R W 2011 Partial angular coherence and the angular schmidt spectrum of entangled two-photon fields *Phys. Rev. A* **84** 063847
[23] Pires H Di L, Florijn H C B and van Exter M P 2010 Measurement of the spiral spectrum of entangled two-photon states *Phys. Rev. Lett.* **104** 020505
[24] Kulkarni G, Sahu R, Magaña-Loaiza O S, Boyd R W and Jha A K 2017 Single-shot measurement of the orbital-angular-momentum spectrum of light *Nat. Commun.* **8** 1054
[25] Kulkarni G, Taneja L, Aarav S and Jha A K 2018 Angular schmidt spectrum of entangled photons: derivation of an exact formula and experimental characterization for noncollinear phase matching *Phys. Rev. A* **97** 063846
[26] Karan S, Van Exter M P and Jha A K 2025 Broadband uniform-efficiency oam-mode detector *Sci. Adv.* **11** eadq7201
[27] Zhou Y, Mirhosseini M, Fu D, Zhao J, Rafsanjani S M H, Willner A E and Boyd R W 2017 Sorting photons by radial quantum number *Phys. Rev. Lett.* **119** 263602
[28] Fu D *et al* 2018 Realization of a scalable laguerre–gaussian mode sorter based on a robust radial mode sorter *Opt. Express* **26** 33057–65
[29] Choudhary S, Sampson R, Miyamoto Y, Magaña-Loaiza O S, Rafsanjani S M H, Mirhosseini M and Boyd R W 2018 Measurement of the radial mode spectrum of photons through a phase-retrieval method *Opt. Lett.* **43** 6101–4
[30] Bouchard F, Valencia N H, Brandt F, Fickler R, Huber M and Malik M 2018 Measuring azimuthal and radial modes of photons *Opt. Express* **26** 31925–41
[31] Offer R F, Stulga D, Riis E, Franke-Arnold S and Arnold A S 2018 Spiral bandwidth of four-wave mixing in Rb vapour *Commun. Phys.* **1** 84
[32] Schneeloch J and Howell J C 2016 Introduction to the transverse spatial correlations in spontaneous parametric down-conversion through the biphoton birth zone *J. Opt.* **18** 053501
[33] Karan S, Aarav S, Bharadhwaj H, Taneja L, De A, Kulkarni G, Meher N and Jha A K 2020 Phase matching in β-barium borate crystals for spontaneous parametric down-conversion *J. Opt.* **22** 083501
[34] Walborn S P, Monken C, Pádua S and Ribeiro P S 2010 Spatial correlations in parametric down-conversion *Phys. Rep.* **495** 87–139

[35] Karan S, Prasad R and Jha A K 2023 Postselection-free controlled generation of a high-dimensional orbital-angular-momentum entangled state *Phys. Rev. Appl.* **20** 054027
[36] Patoary A S M, Kulkarni G and Jha A K 2019 Intrinsic degree of coherence of classical and quantum states *J. Opt. Soc. Am. B* **36** 2765–76
[37] Born M and Wolf E 1999 *Principles of Optics* 7th edn expanded (Cambridge University Press)
[38] Zia D, Dehghan N, D'Errico A, Sciarrino F and Karimi E 2023 Interferometric imaging of amplitude and phase of spatial biphoton states *Nat. Photon.* **17** 1009–16
[39] Jha A K and Boyd R W 2010 Spatial two-photon coherence of the entangled field produced by down-conversion using a partially spatially coherent pump beam *Phys. Rev. A* **81** 013828
[40] Meher N, Patoary A S M, Kulkarni G and Jha A K 2020 Intrinsic degree of coherence of two-qubit states and measures of two-particle quantum correlations *J. Opt. Soc. Am. B* **37** 1224–30
[41] Bhattacharjee A, Biswas S, Alonso M A and Jha A K 2023 Coherence in the radial degree of freedom *J. Opt. Soc. Am. A* **40** 411–6
[42] Prasad R, Senapati N, Karan S, Bhattacharjee A, Piccirillo B, Alonso M A and Jha A K 2025 Experimental technique for measuring radial coherence *Opt. Express* **33** 11693–701
[43] Schneeloch J, Tison C C, Fanto M L, Alsing P M and Howland G A 2019 Quantifying entanglement in a 68-billion-dimensional quantum state space *Nat. Commun.* **10** 2785
[44] Prasad R, Wanare S, Karan S, Joshi M K, Bhattacharjee A and Jha A K 2024 Structured position-momentum-entangled two-photon fields *Phys. Rev. Appl.* **22** 064034
[45] Prevedel R, Hamel D R, Colbeck R, Fisher K and Resch K J 2011 Experimental investigation of the uncertainty principle in the presence of quantum memory and its application to witnessing entanglement *Nat. Phys.* **7** 757–61
[46] Bennett C H, Bernstein H J, Popescu S and Schumacher B 1996 Concentrating partial entanglement by local operations *Phys. Rev. A* **53** 2046